Real-time Risk-averse Dispatch of an Integrated Electricity and Natural Gas System via Conditional Value-at-risk-based Lookup-table Approximate Dynamic Programming

Jianquan Zhu, *Member*, *IEEE*, Guanhai Li, Ye Guo, Jiajun Chen, Haixin Liu, Yuhao Luo, and Wenhao Liu

***Abstract*—The real-time risk-averse dispatch problem of an integrated electricity and natural gas system (IEGS) is studied in this paper. It is formulated as a real-time conditional value-at-risk (CVaR)-based risk-averse dispatch model in the Markov decision process framework. Because of its stochasticity, nonconvexity and nonlinearity, the model is difficult to analyze by traditional algorithms in an acceptable time. To address this non-deterministic polynomial-hard problem, a CVaR-based lookup-table approximate dynamic programming (CVaR-ADP) algorithm is proposed, and the risk-averse dispatch problem is decoupled into a series of tractable subproblems. The line pack is used as the state variable to describe the impact of one period's decision on the future. This facilitates the reduction of load shedding and wind power curtailment. Through the proposed method, real-time decisions can be made according to the current information, while the value functions can be used to overview the whole optimization horizon to balance the current cost and future risk loss. Numerical simulations indicate that the proposed method can effectively measure and control the risk costs in extreme scenarios. Moreover, the decisions can be made within 10 s, which meets the requirement of the real-time dispatch of an IEGS.**

***Index Terms*—Integrated electricity and natural gas system, approximate dynamic programming, real-time dispatch, risk-averse, conditional value-at-risk.**

I. Introduction

The installed capacity of natural gas-fired units in electricity networks has grown rapidly in recent years because of their high efficiency and flexibility [1], [2]. In addition, with the emergence of power-to-gas technology, the coupling between electricity and gas networks is further strengthened [3]. Consequently, as an effective way to enhance energy efficiency, the integrated electricity and natural gas system (IEGS) has attracted wide attention.

To mitigate the dependence on fossil fuels, renewable energy sources have undergone significant developments in IEGS. However, a deep penetration of renewable energy sources in IEGS may pose challenges for its operation. First, the day-ahead dispatch strategies may deviate from the actual cases and even become infeasible in real-time. Hence real-time dispatch strategies become indispensable. Second, during the IEGS operation dispatch process, some decision-makers' attitudes may change from risk neutrality to risk aversion [4]. Therefore, it is necessary to study the risk measure and control technology to assist their real-time decision-making. As a popular risk measurement metric, conditional value-at-risk (CVaR) is widely used for risk aversion in the fields of economics and finance. This motivates the development of a CVaR-based risk-averse method for the real-time dispatch problem of an IEGS.

In order to deal with the IEGS operational uncertainties caused by the high penetration of intermittent renewable energy sources and loads, various methods have been proposed, including stochastic and robust optimization, chance-constrained programming, fuzzy and interval optimization, information gap decision theory methods, and their hybrid methods. Among them, stochastic optimization usually describes the uncertainty by a set of relevant scenarios generated from a known probability distribution [5]. Different from stochastic, robust optimization tends to find a reliable conservative solution, which can avoid the risk, but at the expense of economy [6], [7]. To solve this problem, chance-constrained programming uses the constraint non-violation rate to describe the uncertainty risk [8], and can handle the uncertainty at a given risk level, though it is easy to ignore the tail risk, which widely exists in practice [9]. As one of the mainstream uncertainty handling methods, fuzzy optimization has

Received: March 30, 2023
Accepted: November 4, 2023
Published Online: March 1, 2024
Jianquan Zhu (corresponding author) is with the School of Electric Power Engineering, South China University of Technology, Guangzhou 510640, China (e-mail: zhujianquan@scut.edu.cn).
DOI: 10.23919/PCMP.2023.000247

also been applied in the operation of IEGS. By using fuzzy numbers (e.g., triangular, trapezoidal and Gaussian) to describe the uncertainties, the fuzzy optimization problems can be formulated quantitatively [10]. However, the establishment of membership function is subjective in fuzzy optimization. As a substitute, interval optimization characterizes the uncertainties in the form of intervals and does not need to know the probability distribution or membership function, though it may face a serious interval expansion problem during its calculation processes [11]. Information gap decision theory formulates the uncertainties in the form of a non-probability uncertainty set. By presupposing the worst or best objective according to the maximum fluctuation range of uncertainty, both robustness and economy can be ensured [12]. However, similar to fuzzy optimization, the presupposition of objective in information gap decision theory is subjective. To deal with the drawbacks of the single optimization method, hybrid methods (e.g., hybrid stochastic-fuzzy [10], hybrid stochastic-interval [12], and hybrid robust-stochastic [13]) have also been proposed.

For the real-time operation of an IEGS, there have been various approaches, such as myopic policy and model predictive control (MPC) approaches. Myopic policy simply uses current information to make real-time decisions [14], and since the impact of real-time decisions on future periods is disregarded, it may result in high cost. To solve this problem, MPC uses the forecasting information of several following periods to consider future situations, and thus can provide better results [15]. However, the real-time forecasting information may not be available during the operational process of IEGS in some cases.

To measure the operational risk of an IEGS with uncertainties, the existing methods include value-at-risk (VaR)-based methods, CVaR-based methods, etc. VaR-based methods can quantify the risk loss at a given confidence level α [16], although the tail risk (i.e., the loss beyond the given confidence level) is neglected. To fill this gap, CVaR is proposed in [17], and by taking the conditional probability expected value as the optimization objective, CVaR-based methods can consider the attitudes of decision makers towards the tail risk well. To date, CVaR has been widely applied in various fields, including investment strategy [18], the electricity market [19], and energy management [20]–[22]. The results demonstrate the effectiveness of CVaR in dealing with financial risk. In the field of IEGS, scenario-based CVaR methods have also been successfully applied to handle the risk. For example, CVaR is used to quantify the risk of wind power curtailment and load demand shedding in the energy management of IEGS in [23]. To deal with the uncertainties of wind power and load demand, a scenario-based CVaR framework is established in [24], which can quantize and minimize the impact of the uncertainties from renewable energy power generation and load demand. In [25], CVaR and the interval optimization method are combined to measure the risk brought by the uncertainties in an IEGS. Note that the above CVaR-based methods focus on long-term decision-making problems, in which the time requirement of decision-making is not critical. Theoretically, CVaR is also suitable for the short-term decision-making problem [26]. Therefore, in this paper, CVaR is extended to the real-time dispatch of an IEGS, which helps to measure and control the risk cost in extreme scenarios.

Mathematically, the real-time risk-averse dispatch model of an IEGS with different risk preferences is stochastic, nonconvex and nonlinear. Various algorithms can be used to solve this problem, such as meta-heuristic algorithms, commercial solvers, and dynamic programming (DP)-based algorithms. Classical meta-heuristic algorithms, e.g., genetic algorithm [27], particle swarm optimization [28], and genetic simulating annealing algorithm [29], can deal with an optimization problem with complex mathematical properties. However, meta-heuristic algorithms are sensitive to parameter tuning, and their solution quality is unstable in most cases. Because of their convenience and stability, commercial solvers have become mainstream solution methods for nonlinear programming (NLP) problems in recent years [30]. However, for the stochastic, nonconvex and nonlinear problems, commercial solvers find it difficult to obtain solutions within an acceptable time period. As a powerful optimization algorithm, dynamic programming can decompose the original NLP problem into a series of tractable subproblems [31]. Nevertheless, the traditional DP algorithm depends on discretization, and as the numbers of the discretized state variables and decision variables increase, it will face the challenge of "curse of dimension" [32]. To deal with this issue, the traditional DP algorithm is developed into an approximate dynamic programming (ADP) algorithm. By approximating the exact value function iteratively, the problem of "curse of dimension" can be solved, and ADP has been successfully applied in the fields of energy management [33], [34], the electricity market [35], and optimal planning [36]. To establish the approximate value function, various methods such as piecewise linear functions [37], lookup tables [38], and neural networks [39], can be adopted. Note that the aforementioned ADP algorithms are based on the expected cost-based value functions, and thus they are not suitable to solve the risk-averse decision-making problem.

To solve the risk-averse decision-making problem, a risk-averse DP algorithm is proposed in [40]. Similar to the traditional DP algorithm, the risk-averse DP algorithm faces the challenge of "curse of dimension". In [41], CVaR is further combined with stochastic dual dynamic programming (SDDP), so as to obtain the optimal operation plan of power systems. However, this method is only applicable to linear problems since it

depends on a piecewise-linear outer approximation technique. Moreover, the iterative process of the SDDP algorithm is time-consuming, and it is difficult to meet the requirements of the real-time dispatch of an IEGS.

In this paper, a CVaR-based lookup-table ADP (CVaR-ADP) algorithm is proposed for the real-time risk-averse dispatch of an IEGS. Compared with existing work, the major contributions of this paper are:

1) A CVaR-based risk-averse dispatch model is formulated as a Markov decision process (MDP) for the real-time operation of an IEGS. Then, the decisions can be made period by period, while overviewing the whole optimization horizon to balance current cost and future risk loss effectively.

2) The traditional lookup-table ADP algorithm is developed into a novel CVaR-ADP algorithm. The proposed algorithm is suitable for analyzing the aforementioned risk-averse dispatch model, which represents a non-deterministic polynomial (NP)-hard problem. Moreover, the value functions of CVaR-ADP can be trained offline beforehand. Consequently, both the prediction information and iteration can be avoided, which makes the application convenient and efficient.

The remainder of this paper is structured as follows: Section II establishes the real-time risk-averse dispatch model of an IEGS, and the CVaR-ADP algorithm is proposed to analyze the risk-averse dispatch model in Section III. Numerical simulations are devised to verify the effectiveness of the proposed algorithm in Section IV, and finally, Section V summarizes the conclusions.

II. Real-time Risk-averse Dispatch Model of an IEGS

The configuration of the IEGS studied in this paper is shown in Fig. 1, in which the coupling between the electricity and gas subsystems is realized by natural gas-fired units and power-to-gas (P2G) facilities. In this section, the real-time risk-averse dispatch model of an IEGS is mathematically formulated in the MDP and CVaR frameworks. First, the basic elements (i.e., state and decision variables, exogenous information, state transition functions, and immediate cost) of the MDP are defined.

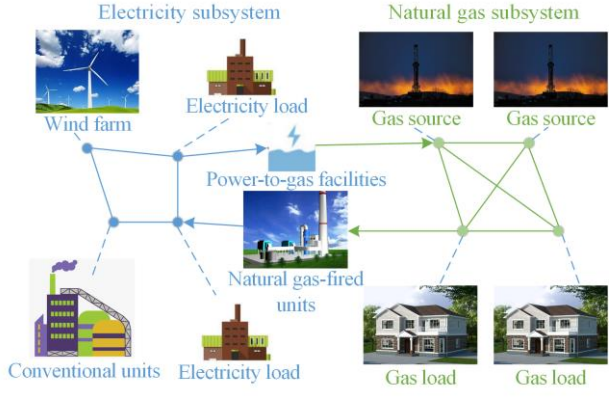

Fig. 1. Configuration of IEGS.

Then, the objective functions and constraints for the real-time risk-averse dispatch of an IEGS are presented.

A. Basic Elements

1) State Variables

The state variables are used to reflect the current states of the IEGS, which are defined as:

$$\boldsymbol{S}_t=\left\{\boldsymbol{P}_{t-\Delta t}^{\mathrm{G}},\boldsymbol{P}_{t-\Delta t}^{\mathrm{NG}},\boldsymbol{P}_{t-\Delta t}^{\mathrm{P2G}},\boldsymbol{P}_t^{\mathrm{W}},\boldsymbol{E}_t^{\mathrm{load}},\boldsymbol{G}_t^{\mathrm{load}},\boldsymbol{G}_{t-\Delta t}^{\mathrm{S}},\boldsymbol{G}_{t-\Delta t}^{\mathrm{L}}\right\},\forall t\in\mathcal{T} \tag{1}$$

where $\boldsymbol{S}_t$ is the state variable vector at period t; $\mathcal{T}$ is the set of periods; $\boldsymbol{P}_{t-\Delta t}^{\mathrm{G}}$, $\boldsymbol{P}_{t-\Delta t}^{\mathrm{NG}}$, and $\boldsymbol{P}_{t-\Delta t}^{\mathrm{P2G}}$ are the active power vectors of conventional units, natural gas-fired units, and P2G facilities at period $(t-\Delta t)$, respectively; $\boldsymbol{P}_t^{\mathrm{W}}$ is the available wind power vector at period t; $\boldsymbol{E}_t^{\mathrm{load}}$ is the electrical load vector at period t; $\boldsymbol{G}_t^{\mathrm{load}}$ is the gas load vector at period t; $\boldsymbol{G}_{t-\Delta t}^{\mathrm{S}}$ is the gas production vector at period $(t-\Delta t)$; and $\boldsymbol{G}_{t-\Delta t}^{\mathrm{L}}$ is the line pack vector at period $(t-\Delta t)$.

2) Decision Variables

In this paper, the decision variables in the real-time risk-averse dispatch of the IEGS are defined as:

$$\boldsymbol{a}_t=\left\{\boldsymbol{P}_t^{\mathrm{G}},\boldsymbol{P}_t^{\mathrm{NG}},\boldsymbol{P}_t^{\mathrm{P2G}},\boldsymbol{P}_t^{\mathrm{WC}},\boldsymbol{E}_t^{\mathrm{LS}},\boldsymbol{G}_t^{\mathrm{LS}},\boldsymbol{G}_t^{\mathrm{S}},\boldsymbol{G}_t^{\mathrm{A}}\right\},\forall t\in\mathcal{T} \tag{2}$$

where $\boldsymbol{a}_t$ is the decision variable vector at period t; $\boldsymbol{P}_t^{\mathrm{G}}$, $\boldsymbol{P}_t^{\mathrm{NG}}$, and $\boldsymbol{P}_t^{\mathrm{P2G}}$ are the active power vectors of conventional units, natural gas-fired units, and P2G facilities at period t, respectively; $\boldsymbol{P}_t^{\mathrm{WC}}$ and $\boldsymbol{E}_t^{\mathrm{LS}}$ are the wind power curtailment vector and electrical load shedding vector at period t, respectively; $\boldsymbol{G}_t^{\mathrm{LS}}$ is the gas load shedding vector at period t; $\boldsymbol{G}_t^{\mathrm{S}}$ is the gas production vector at period t; and $\boldsymbol{G}_t^{\mathrm{A}}$ is the line pack change vector at period t.

3) Exogenous Information

The exogenous information is used to describe the stochastic factors of the IEGS, and is defined as $\boldsymbol{W}_t$:

$$\boldsymbol{W}_t=\left\{\hat{\boldsymbol{P}}_t^{\mathrm{W}},\hat{\boldsymbol{E}}_t^{\mathrm{load}},\hat{\boldsymbol{G}}_t^{\mathrm{load}}\right\},\forall t\in\mathcal{T} \tag{3}$$

where $\hat{\boldsymbol{P}}_t^{\mathrm{W}}$, $\hat{\boldsymbol{E}}_t^{\mathrm{load}}$ and $\hat{\boldsymbol{G}}_t^{\mathrm{load}}$ are the prediction random errors of wind power, electricity and gas load demands, respectively. As with [37], they are uniformly described by a Gaussian distribution in this paper.

4) State Transition Functions

The state transition function is used to describe the state relationship between two adjacent periods with the given decision $\boldsymbol{a}_t$ at the exogenous information $\boldsymbol{W}_{t+\Delta t}$:

$$\boldsymbol{S}_{t+\Delta t}=\boldsymbol{S}^{\mathrm{M}}\left(\boldsymbol{S}_t,\boldsymbol{a}_t,\boldsymbol{W}_{t+\Delta t}\right),\forall t\in\mathcal{T} \tag{4}$$

where $\boldsymbol{S}^{\mathrm{M}}(\cdot)$ is the state transition function. Specifically, the state transition functions are defined as:

$$\boldsymbol{P}_{t+\Delta t}^{\mathrm{W}}=\boldsymbol{P}_t^{\mathrm{W}}+\hat{\boldsymbol{P}}_{t+\Delta t}^{\mathrm{W}},\forall t\in\mathcal{T} \tag{5}$$

$$\boldsymbol{E}_{t+\Delta t}^{\mathrm{load}}=\boldsymbol{E}_t^{\mathrm{load}}+\hat{\boldsymbol{E}}_{t+\Delta t}^{\mathrm{load}},\forall t\in\mathcal{T} \tag{6}$$

$$\boldsymbol{G}_{t+\Delta t}^{\mathrm{load}}=\boldsymbol{G}_t^{\mathrm{load}}+\hat{\boldsymbol{G}}_{t+\Delta t}^{\mathrm{load}},\forall t\in\mathcal{T} \tag{7}$$

$$\boldsymbol{G}_{t+\Delta t}^{\mathrm{L}}=\boldsymbol{G}_{t}^{\mathrm{L}}+\boldsymbol{G}_{t}^{\mathrm{A}},\forall t\in\mathcal{T} \tag{8}$$

$$\boldsymbol{G}_{t}^{\mathrm{A}}=x\Delta\boldsymbol{G}_{t}^{\mathrm{L}},\forall t\in\mathcal{T} \tag{9}$$

$$\Delta\boldsymbol{G}_{t}^{\mathrm{L}}=\frac{\boldsymbol{G}_{\max}^{\mathrm{L}}-\boldsymbol{G}_{\min}^{\mathrm{L}}}{D},\forall t\in\mathcal{T} \tag{10}$$

where x is the integer variable used for discretization; $\Delta\boldsymbol{G}_{t}^{\mathrm{L}}$ is the unit discretized value of line pack; $\boldsymbol{G}_{\max}^{\mathrm{L}}$ and $\boldsymbol{G}_{\min}^{\mathrm{L}}$ are the maximum and minimum values of line pack; and D is the number of discrete segments.

5) Immediate Cost

The immediate cost of an IEGS includes the operational, penalty and maintenance costs, which can be described as:

$$\begin{aligned}C_t(\boldsymbol{S}_t,\boldsymbol{a}_t)=&\sum_{m\in\mathcal{S}(m)}\mu_m G_{m,t}^{\mathrm{S}}+\sum_{i\in\mathcal{C}(i)}(a_i(P_{i,t}^{\mathrm{G}})^2+b_i P_{i,t}^{\mathrm{G}}+c_i)+\\&\sum_{m\in\mathcal{G}(m)}C_g^{\mathrm{P}}G_{m,t}^{\mathrm{LS}}+\sum_{i\in\mathcal{E}(i)}C_e^{\mathrm{P}}P_{i,t}^{\mathrm{LS}}+\sum_{i\in\mathcal{W}(i)}C_w^{\mathrm{P}}P_{i,t}^{\mathrm{WC}}+\\&\sum_{m,n\in\mathcal{L}(m)}C_{m,n}(G_{m,n,t}^{\mathrm{L}}-G_{m,n,0}^{\mathrm{L}}),\forall t\in\mathcal{T}\end{aligned} \tag{11}$$

where $C_t(\cdot)$ is the immediate cost function at period t; $\mathcal{S}(m)$, $\mathcal{C}(i)$, $\mathcal{G}(m)$, $\mathcal{E}(i)$, $\mathcal{W}(i)$, and $\mathcal{L}(m)$ are sets of gas sources, convention units, gas loads, electrical loads, wind farms, and pipelines, respectively; μ_m is the unit production cost of gas source m; $G_{m,t}^{\mathrm{S}}$ is the gas production of gas source m at period t; a_i, b_i, and c_i are the cost coefficients of conventional unit i; $P_{i,t}^{\mathrm{G}}$ is the active power of conventional unit i at period t; $C_{\mathrm{g}}^{\mathrm{P}}$, $C_{\mathrm{e}}^{\mathrm{P}}$, and $C_{\mathrm{w}}^{\mathrm{P}}$ are the penalty coefficients of gas load shedding, electrical load shedding, and wind power curtailment, respectively; $G_{m,t}^{\mathrm{LS}}$ is the load shedding of gas load m at period t; $P_{i,t}^{\mathrm{LS}}$ is the load shedding of electrical load i at period t; $P_{i,t}^{\mathrm{WC}}$ is the wind power curtailment of wind farms i at period t; $C_{m,n}$ is the unit line pack maintain cost of pipeline mn; $G_{m,n,t}^{\mathrm{L}}$ is the line pack of pipeline mn at period t; and $G_{m,n,0}^{\mathrm{L}}$ is the line pack of pipeline mn at period 0.

In (11), the first and second terms represent the operational costs of gas sources and conventional units (i.e., coal-fired units), respectively. The third, fourth and fifth terms represent the respective penalty costs of gas and electricity load shedding, and wind power curtailment. These are used to prevent load shedding and promote wind power consumption. The final term represents the maintenance cost of the pipeline.

B. Objective Function

Generally, the dispatch objective of an IEGS is to minimize the expectation of the operational cost across the entire optimization horizon, i.e.: $\min E\left[\sum_{t\in\mathcal{T}}C_t(\boldsymbol{S}_t,\boldsymbol{a}_t)\right]$.

According to Bellman's equation, the objective function can be described as:

$$V_t(\boldsymbol{S}_t)=\min_{\boldsymbol{a}_t\in\mathcal{A}}\left\{C_t(\boldsymbol{S}_t,\boldsymbol{a}_t)+E\left[V_{t+\Delta t}(\boldsymbol{S}_{t+\Delta t})\middle|\boldsymbol{S}_t\right]\right\} \tag{12}$$

$$V_{t+\Delta t}(\boldsymbol{S}_{t+\Delta t})=\sum_{\tau=t+\Delta t}^{T}C_\tau(\boldsymbol{S}_\tau,\boldsymbol{a}_\tau) \tag{13}$$

where $V_t(\boldsymbol{S}_t)$ is the value function of state variable $\boldsymbol{S}_t$; $V_{t+\Delta t}(\boldsymbol{S}_{t+\Delta t})|\boldsymbol{S}_t$ is the conditional value function of $\boldsymbol{S}_{t+\Delta t}$ and represents the optimal total cost of the subsequent periods; while $E(\cdot)$ represents the expectation operator.

Although the expectation minimization model is economical in most cases, it usually ignores the high-cost risk in rare critical scenarios. In order to solve this problem, a CVaR-based real-time risk-averse model is employed.

CVaR is an effective risk measurement developed on the basis of VaR. The relationship between CVaR and VaR is illustrated in Fig. 2, in which VaR(α) describes the maximum cost loss under the confidence level α, i.e., the quantile of cost under the confidence level α, while CVaR(α) represents the average value of exceeding this quantile. Considering VaR(α) cannot illustrate the cost loss beyond the confidence level α, the tail of the probability distribution is taken into consideration as an addition. In this way, the cost loss exceeding the confidence level can also be evaluated. This helps to reduce the cost loss in rare critical scenarios.

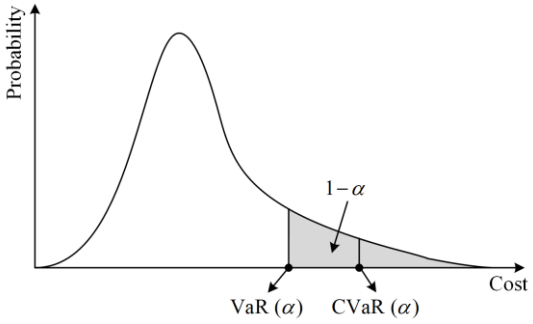

Fig. 2. The relationship between CVaR and VaR.

According to the CVaR theory and the Bellman optimality principle, equation (12) can be reconstructed using CVaR-based Bellman's equation as:

$$V_t(\boldsymbol{S}_t)=\min_{\boldsymbol{a}_t\in\mathcal{A}}\left\{\rho_t^{\lambda_t}(C_t)+\rho_{t+\Delta t}^{\lambda_{t+\Delta t}}\left[V_{t+\Delta t}(\boldsymbol{S}_{t+\Delta t})\middle|\boldsymbol{S}_t\right]\right\} \tag{14}$$

$$\rho_t^{\lambda_t}(C_t)=(1-\beta_t)E(C_t)+\beta_t R_{\alpha_t}^{\mathrm{CVaR}}(C_t) \tag{15}$$

where $\rho_t^{\lambda_t}(C_t)$ is the risk measure value for the immediate cost; $\lambda_t=(\alpha_t,\beta_t)$ is the risk-averse preference parameter, which refers to the risk-averse level of the decision-maker (i.e., the operator of the IEGS);

$\alpha_t \in (0,1)$ is the confidence level; $\beta_t \in (0,1)$ is the weighted coefficient of $R_{\alpha_t}^{\mathrm{CVaR}}$; $E(C_t)$ and $R_{\alpha_t}^{\mathrm{CVaR}}$ are the respective expectation and tail risk value of the immediate cost. These can be calculated by:

$$R_{\alpha_t}^{\mathrm{CVaR}}(C_t) = \min\{\xi_{\alpha_t} + \frac{1}{1-\alpha_t} E[\max\{C_t - \xi_{\alpha_t}, 0\}]\} \quad (16)$$

$$\xi_{\alpha_t} = \min_{\xi_{\alpha_t}} \{\mathrm{P}(C_t \leqslant \xi_{\alpha_t}) \geqslant \alpha_t\} \quad (17)$$

where ξ_{α_t} is the VaR of C_t at the confidence level α_t.

In (14)–(17), the confidence level α represents the occurrence probability of extreme scenarios, and the weight β represents the trade-off between the average cost and realized cost of extreme scenarios. These risk preference parameters reflect the attitude of the decision-makers. For example, a larger value of β means that the decision-maker places a greater emphasis on avoiding potential losses or negative outcomes of tail-risk events. Consequently, decision-making result of the proposed method will become more conservative. In addition, the tail risk specifically refers to the potential losses or negative outcomes of tail-risk events caused by wind power curtailment and load demand shedding.

C. Constraints

The decision process is subjected to the following constraints [42]–[44].

1) Operating Constraints of Electricity Subsystem

$$\left| \sum_{b \in B(b)} \boldsymbol{A}_{lb} \begin{bmatrix} \sum_{i \in C(i)} P_{i,t}^{\mathrm{G}} + \sum_{i \in N(i)} P_{i,t}^{\mathrm{NG}} - \sum_{i \in E(i)} (E_{i,t}^{\mathrm{load}} - E_{i,t}^{\mathrm{LS}}) \\ - \sum_{i \in P(i)} P_{i,t}^{\mathrm{P2G}} + \sum_{i \in W(i)} (P_{i,t}^{\mathrm{W}} - P_{i,t}^{\mathrm{WC}}) \end{bmatrix} \right| \leqslant P_{l,\max}^{\mathrm{L}}, \forall t \in \mathcal{T} \quad (18)$$

$$\sum_{i \in C(i)} P_{i,t}^{\mathrm{G}} + \sum_{i \in N(i)} P_{i,t}^{\mathrm{NG}} + \sum_{i \in W(i)} (P_{i,t}^{\mathrm{W}} - P_{i,t}^{\mathrm{WC}}) = \sum_{i \in E(i)} (E_{i,t}^{\mathrm{load}} - E_{i,t}^{\mathrm{LS}}) + \sum_{i \in P(i)} P_{i,t}^{\mathrm{P2G}}, \forall t \in \mathcal{T} \quad (19)$$

$$P_{i,\min}^{\mathrm{G}} \leqslant P_{i,t}^{\mathrm{G}} \leqslant P_{i,\max}^{\mathrm{G}}, \forall i \in C(i), \forall t \in \mathcal{T} \quad (20)$$

$$P_{i,\min}^{\mathrm{NG}} \leqslant P_{i,t}^{\mathrm{NG}} \leqslant P_{i,\max}^{\mathrm{NG}}, \forall i \in N(i), \forall t \in \mathcal{T} \quad (21)$$

$$0 \leqslant P_{i,t}^{\mathrm{P2G}} \leqslant P_{i,t}^{\mathrm{W}}, \forall i \in P(i), \forall t \in \mathcal{T} \quad (22)$$

$$0 \leqslant P_{i,t}^{\mathrm{WC}} \leqslant P_{i,t}^{\mathrm{W}}, \forall i \in W(i), \forall t \in \mathcal{T} \quad (23)$$

$$0 \leqslant E_{i,t}^{\mathrm{LS}} \leqslant E_{i,t}^{\mathrm{load}}, \forall i \in E(i), \forall t \in \mathcal{T} \quad (24)$$

where $P_{l,\max}^{\mathrm{L}}$ is the maximum transmission power of line l; $B(b)$ is the set of electrical buses; $\boldsymbol{A}_{lb}$ is the power transfer matrix, which represents the impact of the injected power of bus b on line l; $P_{i,t}^{\mathrm{NG}}$ is the active power of natural gas-fired unit i at period t; $P_{i,t}^{\mathrm{load}}$ is the electrical load demand of electrical bus i at period t; $P_{i,t}^{\mathrm{LS}}$ is the load shedding of electrical load i at period t; $P_{i,t}^{\mathrm{P2G}}$ is the active power of P2G facilitie i at period t; $P_{l,\max}^{\mathrm{L}}$ is the maximum transmission power of line l; $P(i)$ and $N(i)$ are sets of P2G facilities and natural gas-fired units, respectively; $P_{i,t}^{\mathrm{W}}$ is the available wind power wind farms i at period t; $P_{i,\min}^{\mathrm{G}}$ and $P_{i,\max}^{\mathrm{G}}$ are the lower and upper limits of the active power generations of conventional unit i; $P_{i,\min}^{\mathrm{NG}}$ and $P_{i,\max}^{\mathrm{NG}}$ are the lower and upper limits of the active power generations of natural gas-fired unit i.

Equation (18) describes the branch power flow constraints, and (19) describes the power balance constraints. Equations (20)–(22) describe the output limits of conventional units, natural gas-fired units, and P2G facilities, respectively, whereas (23) and (24) describe the limits of wind power curtailment and electricity load shedding, respectively.

2) Operating Constraints of Gas Subsystem

$$\sum_{m \in S(m)} G_{m,t}^{\mathrm{S}} - \sum_{m \in G(m)} (G_{m,t}^{\mathrm{load}} - G_{m,t}^{\mathrm{LS}}) - \sum_{m \in V(m)} G_{m,t}^{\mathrm{G2P}} + \sum_{m \in K(m)} G_{m,t}^{\mathrm{P2G}} = \sum_{m \in L(m)} F_{m,n,t}, \forall m \in L(m), \forall t \in \mathcal{T} \quad (25)$$

$$\bar{F}_{m,n,t}^2 = W_{m,n}(\pi_{m,t}^2 - \pi_{n,t}^2), \forall m,n \in L(m), \forall t \in \mathcal{T} \quad (26)$$

$$\bar{F}_{mn,t} = 1/2(F_{mn,t} - F_{nm,t}), \forall m,n \in L(m), \forall t \in \mathcal{T} \quad (27)$$

$$\pi_m^{\min} \leqslant \pi_{m,t} \leqslant \pi_m^{\max}, \forall m \in L(m), \forall t \in \mathcal{T} \quad (28)$$

$$G_{m,\min}^{\mathrm{S}} \leqslant G_{m,t}^{\mathrm{S}} \leqslant G_{m,\max}^{\mathrm{S}}, \forall m \in S(m), \forall t \in \mathcal{T} \quad (29)$$

$$0 \leqslant G_{m,t}^{\mathrm{LS}} \leqslant G_{m,t}^{\mathrm{load}}, \forall m \in G(m), \forall t \in \mathcal{T} \quad (30)$$

where $G_{m,t}^{\mathrm{load}}$ is the gas load demand of gas node m at period t; $G_{m,t}^{\mathrm{NG}}$ is the gas consumption of the natural gas-fired unit connected to node m at period t; $K(m)$ and $V(m)$ are sets of P2G facilities and natural gas-fired units connected to node m, respectively; $G_{m,t}^{\mathrm{P2G}}$ is the gas production of the P2G facility connected to node m at period t; $W_{m,n}$ is the Weymouth constant of pipeline mn; $\pi_{m,t}$ and $\pi_{n,t}$ is the gas pressure of node m and node n at period t, respectively; $\bar{F}_{m,n,t}$ is the average gas flow through pipeline mn at period t; $F_{m,n,t}$ is the gas flow injected from node m to node n at period t; $F_{n,m,t}$ is the gas flow injected from node n to node m at period t; $\pi_m^{\min}$ and $\pi_m^{\max}$ are the lower and upper limits of the gas pressure of node m; $G_{m,\min}^{\mathrm{S}}$ and $G_{m,\max}^{\mathrm{S}}$ are the lower and upper limits of the gas production of gas source m.

Equation (25) describes the gas flow balance constraints, while (26) and (27) describe the relationship between the nodal pressure and gas flow. Equations (28)–(30) describe the limits of nodal pressure, gas production, and gas load shedding, respectively.

3) Operating Constraints of Line Pack

$$G_{m,n,t}^{\mathrm{L}} = 1/2K_{m,n}(\pi_{m,t} + \pi_{n,t}), \forall m,n \in L(m), \forall t \in \mathcal{T} \quad (31)$$

$$G_{m,n,t}^{\mathrm{L}} - G_{m,n,t-\Delta t}^{\mathrm{L}} = (F_{m,n,t} + F_{n,m,t})\Delta t, \forall m,n \in L(m), \forall t \in \mathcal{T} \quad (32)$$

$$G_{\min}^{\mathrm{L}} \leqslant \sum_{m,n \in L(m)} G_{m,n,t}^{\mathrm{L}} \leqslant G_{\max}^{\mathrm{L}}, \forall t \in \mathcal{T} \quad (33)$$

$$G_t^{\mathrm{A}} = \sum_{m \in S(m)} G_{m,t}^{\mathrm{S}} + \sum_{m \in K(m)} G_{m,t}^{\mathrm{P2G}} - \sum_{m \in G(m)} (G_{m,t}^{\mathrm{load}} - G_{m,t}^{\mathrm{LS}}) - \sum_{m \in V(m)} G_{m,t}^{\mathrm{G2P}}, \forall t \in \mathcal{T} \quad (34)$$

where $W_{m,n}$ is the Weymouth constant of pipeline *mn*; $F_{n,m,t}$ is the gas flow injected from node *n* to node *m* at period *t*; $G_{m,n,t}^{\mathrm{L}}$ is the line pack of pipeline *mn* at period *t*; $G_{\min}^{\mathrm{L}}$ and $G_{\max}^{\mathrm{L}}$ are the lower and upper limits of the line pack of pipeline; G_t^{A} is the line pack change at period *t*; $G_{m,t}^{\mathrm{NG}}$ is the gas consumption of the natural gas-fired unit connected to node *m* at period *t*; $G_{m,t}^{\mathrm{P2G}}$ is the gas production of the P2G facility connected to node *m* at period *t*; $K_{m,n}$ is line pack parameter of pipeline *mn* at period *t*; and $G_{m,n,t}^{\mathrm{L}}$ is the line pack of pipeline *mn* at period *t*.

Equations (31) and (32) describe the relationship between nodal pressure and line pack, equation (33) describes the upper and lower bounds of line pack, and (34) describes the change of line pack.

4) Operating Constraints of Coupling Facility

The coupling facilities include natural gas-fired units and P2G facilities, whose operational characteristics can be described respectively as:

$$G_{m,t}^{\mathrm{NG}} = \eta_{\mathrm{NG}} P_{m,t}^{\mathrm{NG}}, \forall m \in N(m), \forall t \in \mathcal{T} \quad (35)$$

$$G_{m,t}^{\mathrm{P2G}} = \eta_{\mathrm{P2G}} P_{m,t}^{\mathrm{P2G}}, \forall m \in K(m), \forall t \in \mathcal{T} \quad (36)$$

where η_{NG} and η_{P2G} are the conversion coefficients of the natural gas-fired units and P2G facilities, respectively; $N(m)$ and $K(m)$ are sets of nodes including gas-fired units and P2G facilities, respectively; $G_{m,t}^{\mathrm{NG}}$ is the gas consumption of the natural gas-fired unit connected to node *m* at period *t*; $P_{m,t}^{\mathrm{NG}}$ is the active power of the natural gas-fired unit connected to node *m* at period *t*; $P_{m,t}^{\mathrm{P2G}}$ is the active power of the P2G facility connected to node *m* at period *t*; and $N(m)$ and $K(m)$ are sets of nodes including gas-fired units and P2G facilities, respectively.

III. CVaR-ADP Algorithm

Due to stochastic, nonconvex, and nonlinear properties, the real-time risk-averse dispatch model of an IEGS is difficult to analyze by traditional algorithms in an acceptable time. As an effective optimization method, ADP is able to decompose the complex problem into a series of small problems. However, the traditional ADP algorithm, which takes the minimum expected cost as the optimization objective, is not suitable for the above risk-averse dispatch model. In order to deal with this problem, the traditional ADP algorithm is developed into the CVaR-ADP algorithm in this section.

A. Formulation of CVaR-VF

In (14), the value function is the key to solving the real-time risk-averse dispatch problem. Since the real value function is unknown, it needs to be approached by the approximate value function. The commonly used approximate value functions include look-up tables and piecewise-linear functions. However, they cannot be directly applied to (14), which includes the CVaR cost at a given confidence level. In order to solve this problem, a new CVaR-based value function (CVaR-VF) is proposed.

Similar to the look-up table-based approximate value function, the CVaR-VF is described as:

$$\bar{V}_t^{\mathrm{CVaR}}(\hat{\boldsymbol{S}}_t) = \min_{\hat{\boldsymbol{a}}_t \in \mathcal{A}} \left\{ \rho_t^{\lambda_t}(C_t) + \rho_{t+\Delta t}^{\lambda_{t+\Delta t}} \left[\bar{V}_{t+\Delta t}^{\mathrm{CVaR}}(\hat{\boldsymbol{S}}_{t+\Delta t}) \middle| \hat{\boldsymbol{S}}_t \right] \right\} \quad (37)$$

where $\bar{V}_t^{\mathrm{CVaR}}(\cdot)$ and $\bar{V}_{t+\Delta t}^{\mathrm{CVaR}}(\cdot)$ are the CVaR-VF at period *t* and $(t-\Delta t)$, respectively; $\mathcal{A}$ is the set of feasible decision; while $\hat{\boldsymbol{S}}_t$ and $\hat{\boldsymbol{a}}_t$ are the discretized state variables and decision variables, respectively, which can be obtained by:

$$\Delta Z = (Z_{\max} - Z_{\min})/d_Z \quad (38)$$

$$\hat{Z} \in \{Z_{\min}, Z_{\min} + \Delta Z, Z_{\min} + 2\Delta Z, \cdots, Z_{\max} - \Delta Z, Z_{\max}\} \quad (39)$$

where *Z* represents the element in $\boldsymbol{S}_t$ and $\boldsymbol{a}_t$; ΔZ represents the unit discretized value of *Z*; d_Z represents the number of discrete segments of *Z*; and $\hat{Z}$ represents the discretized *Z*.

To tackle the problem of "curse of dimension" in the information space, the post-decision state proposed in [36] is introduced and (37) can be rewritten as:

$$\bar{V}_{t-\Delta t}^{\mathrm{CVaR},a}(\boldsymbol{S}_{t-\Delta t}^a) = \min_{\boldsymbol{a}_t} \left\{ \rho_t^{\lambda_t}(C_t(\boldsymbol{S}_{t-\Delta t}^a, \boldsymbol{a}_t, \boldsymbol{W}_t)) + \bar{V}_t^{\mathrm{CVaR},a}(\boldsymbol{S}_t^a) \right\} \quad (40)$$

where $\bar{V}_{t-\Delta t}^{\mathrm{CVaR},a}(\cdot)$ is the CVaR-VF of the post-decision state; and $\boldsymbol{S}_t^a$ is the post-decision state. The physical meaning of (40) is the impact of the current decisions on the subsequent periods, i.e., the sum of CVaR cost of the subsequent periods.

In (40), $\rho_t^{\lambda_t}(C_t(\boldsymbol{S}_{t-\Delta t}^a, \boldsymbol{a}_t, \boldsymbol{W}_t))$ and $\bar{V}_t^{\mathrm{CVaR},a}(\boldsymbol{S}_t^a)$ should be calculated period by period. The details are presented in the following two subsections.

B. Calculation of CVaR Immediate Cost

In (40), the CVaR immediate cost $\rho_t^{\lambda_t}(C_t(\boldsymbol{S}_{t-\Delta t}^a, \boldsymbol{a}_t, \boldsymbol{W}_t))$ can be specifically described as:

$$\rho_t^{\lambda_t}(C_t(\boldsymbol{S}_{t-\Delta t}^a,\boldsymbol{a}_t,\boldsymbol{W}_t))=(1-\beta_t)E(C_t(\boldsymbol{S}_{t-\Delta t}^a,\boldsymbol{a}_t,\boldsymbol{W}_t))+\beta_t R_{\alpha_t}^{\mathrm{CVaR}}(C_t(\boldsymbol{S}_{t-\Delta t}^a,\boldsymbol{a}_t,\boldsymbol{W}_t)) \tag{41}$$

From [16], Monte Carlo (MC) sampling is employed to respectively approximate $E(C_t(\boldsymbol{S}_{t-\Delta t}^a,\boldsymbol{a}_t,\boldsymbol{W}_t))$ and $R_{\alpha_t}^{\mathrm{CVaR}}(C_t(\boldsymbol{S}_{t-\Delta t}^a,\boldsymbol{a}_t,\boldsymbol{W}_t))$ as:

$$E(C_t(\boldsymbol{S}_{t-\Delta t}^a,\boldsymbol{a}_t,\boldsymbol{W}_t))=\frac{1}{M}\left(\sum_{s=1}^{M}C_t(\boldsymbol{S}_{t-\Delta t}^a,\boldsymbol{a}_t,\boldsymbol{W}_t^s)\right) \tag{42}$$

$$R_{\alpha_t}^{\mathrm{CVaR}}(C_t(\boldsymbol{S}_{t-\Delta t}^a,\boldsymbol{a}_t,\boldsymbol{W}_t))=\min\left\{\xi_{\alpha_t}+\frac{1}{(1-\alpha_t)M}\sum_{s=1}^{M}\max\left\{C_t(\boldsymbol{S}_{t-\Delta t}^a,\boldsymbol{a}_t,\boldsymbol{W}_t^s)-\xi_{\alpha_t},0\right\}\right\} \tag{43}$$

where M is the number of MC sampling scenarios; W_t^s is the exogenous information vector of scenario s; and $C_t(\boldsymbol{S}_{t-\Delta t}^a,\boldsymbol{a}_t,\boldsymbol{W}_t^s)$ is the immediate cost of the sth scenario at period t.

As long as the immediate cost of each scenario is substituted into (42), $E(C_t(\boldsymbol{S}_{t-\Delta t}^a,\boldsymbol{a}_t,\boldsymbol{W}_t))$ can be directly calculated.

For calculating $R_{\alpha_t}^{\mathrm{CVaR}}(C_t(\boldsymbol{S}_{t-\Delta t}^a,\boldsymbol{a}_t,\boldsymbol{W}_t))$, the bi-level optimization problem described in (43) is handled using the approximate method proposed in [45]. First, the auxiliary variables are introduced to replace the inner-layer problem of (43) as:

$$\eta_{s,t}=\max\left\{C_t(\boldsymbol{S}_{t-\Delta t}^a,\boldsymbol{a}_t,\boldsymbol{W}_t^s)-\xi_{\alpha_t},0\right\} \tag{44}$$

where $\eta_{s,t}$ is the auxiliary variable of the sth scenario at period t.

Then, equation (43) can be transformed to the tractable single-level optimization problem as:

$$R_{\alpha_t}^{\mathrm{CVaR}}(C_t(\boldsymbol{S}_{t-\Delta t}^a,\boldsymbol{a}_t,\boldsymbol{W}_t^s))=\min\left\{\xi_{\alpha_t}+\frac{1}{(1-\alpha_t)M}\sum_{s=1}^{M}\eta_{s,t}\right\} \tag{45}$$

$$\text{s.t. } C_t(\boldsymbol{S}_{t-\Delta t}^a,\boldsymbol{a}_t,\boldsymbol{W}_t^s)-\xi_{\alpha_t}\leqslant\eta_{s,t}\quad\forall s,t \tag{46}$$

$$\eta_{s,t}\geqslant 0\quad\forall s,t \tag{47}$$

C. Update of CVaR-VF

In (40), the CVaR-VF $\bar{V}_t^{\mathrm{CVaR},a}(\cdot)$ should be iteratively updated through the following two processes, while the update principle of CVaR-VF is depicted in Fig. 3.

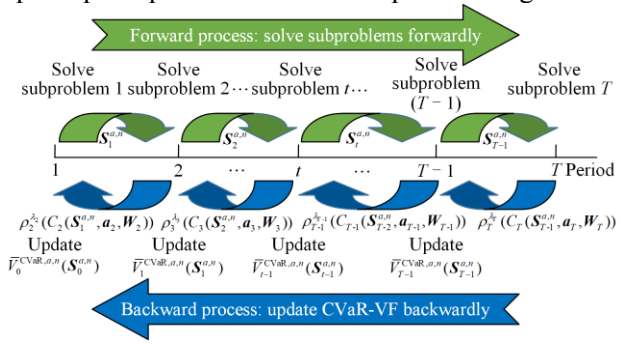

Fig. 3. Update principle of the CVaR-VF.

1) Forward Process

The forward process aims to obtain the CVaR immediate cost of each period by solving (40) from period 1 to period T. Then, the post-decision state variables of current period t are passed to subproblem $(t+\Delta t)$, which is used to update its state in the next iteration. Note that when solving subproblem (40) in the forward process, the decision variables are known in advance, according to which the feasible decision is traversed to obtain a better one.

2) Backward Process

The backward process aims to update CVaR-VF by recursively solving (40) from period T to period 1. Then, the CVaR-VF of current period t is passed to subproblem $(t-\Delta t)$. This helps to update its decision in the next iteration.

According to [46], the iteration process should stop when one of the convergence conditions is satisfied, i.e., the maximum training number is reached or the following tolerance of CVaR-VF is met:

$$\left|\bar{V}_t^{\mathrm{CVaR},a,n}(\boldsymbol{S}_t^{a,n})-\bar{V}_t^{\mathrm{CVaR},a,n-1}(\boldsymbol{S}_t^{a,n})\right|\leqslant\varepsilon,\forall t \tag{48}$$

where $\bar{V}_t^{\mathrm{CVaR},a,n-1}(\boldsymbol{S}_t^{a,n})$ is the value of $\bar{V}_t^{\mathrm{CVaR},a,n}(\boldsymbol{S}_t^{a,n})$ in the $(n-1)$th iteration.

The update process of CVaR-VF is summarized as algorithm 1, which is shown in Table I.

TABLE I
ALGORITHM 1. UPDATE OF CVAR-VF

Algorithm 1. Update of CVaR-VF

1: **Initialization:** Initialize the maximum training number N, the convergence tolerance ε, the optimization horizon $\mathcal{T}$, and the discrete segments of variable d_z.
2: Set the training index $n=1$ and the optimization interval $\Delta t=1$.
3: **Solve subproblems forwards**
for $t=1,2,\cdots,T$
1) Enumerate the feasible decisions in the feasible decision space $\mathcal{A}_t$ constructed by (18)–(36);
3) Solve subproblem (40) subjected to (9), (11), (18)–(36), and (44)–(48);
4) Record $\boldsymbol{a}_t^{n,*}$ and $\rho_t^{\lambda_t}(C_t(\boldsymbol{S}_{t-\Delta t}^{a,n},\boldsymbol{a}_t^{n*},\boldsymbol{W}_t^n))$;
5) Step into the next state according to (5)–(8).
end for
4: **Update value functions backwards**
for $t=T,T-1,\cdots,1$
1) Receive $\rho_t^{\lambda_t}(C_t(\boldsymbol{S}_{t-\Delta t}^{a,n},\boldsymbol{a}_t^{n*},\boldsymbol{W}_t^n))$;
2) Update $\bar{V}_{t-\Delta t}^{\mathrm{CVaR},a,n}(\boldsymbol{S}_{t-\Delta t}^{a,n})$ according to (41).
end for
5: Let $n=n+1$.
6: **Check convergence**
1) If $n=N$ or (49) is satisfied, terminate the update process, and return $\bar{V}_t^{\mathrm{CVaR},a,n}(\boldsymbol{S}_t^a)$;
2) Otherwise, go to Step 3.

D. Procedure of the Proposed Algorithm

In Algorithm 1, the update of CVaR-VF is time-consuming, and it is difficult to satisfy the real-time operational requirement of an IEGS. To handle this problem, the value functions are trained offline in this

subsection. When large numbers of scenarios are considered in this offline training process, we can consider that the value function has been embedded with enough empirical knowledge [37]. Then, these well-trained value functions can be applied to the real-time dispatch, which facilitates the acceleration of the decision-making procedure in the real-time risk-averse dispatch stage.

The procedure of the CVaR-ADP algorithm with the offline training process is outlined as algorithm 2, which is shown in Table II.

TABLE II
ALGORITHM 2. PROCEDURE OF CVAR-ADP

Algorithm 2. Procedure of CVaR-ADP

Stage I: Offline value function training procedure

1: **Initialization:** Initialize the state $\boldsymbol{S}_1$, and choose the risk-averse preference.

2: **Input** the distribution information (i.e., mean and standard deviations) of the prediction errors of gas load, electricity load, and wind power.

3: **Sample** M training scenarios by the MC method.

4: **Obtain** the $\bar{V}_t^{\mathrm{CVaR},a,n}(\boldsymbol{S}_t^a)$ according to Algorithm 1.

Stage II: Real-time optimization dispatch procedure

1: **Input** the well-trained $\bar{V}_t^{\mathrm{CVaR},a,n}(\boldsymbol{S}_t^a)$ obtained from stage I.

2: **for** $t=1,2,\cdots,T$

1) Obtain the real-time electricity load demand, gas load demand, and wind power generation;

2) Solve (41) subjected to (9), (11), (18)–(36), and (42)–(48), and obtain the near-optimal decision $\boldsymbol{a}_t^*$;

3) Execute decision $\boldsymbol{a}_t^*$ and step into the next state according to (5)–(8).

3: **end for**

Similar to [34] and [38], when solving (40), the optimality in theory cannot be guaranteed because of the nonconvexity and nonlinearity of the problem. However, the proposed algorithm can provide satisfactory solutions in all the practices.

IV. NUMERICAL ANALYSIS

In this section, the effectiveness of the proposed method is tested by numerical cases on a 4-bus-4-node IEGS [43] and a modified IEEE-39-bus-Belgian-20-node IEGS [44]. The optimization horizon $\mathcal{T}$ is set to 24 h, and the risk-averse preferences at different periods are set to be the same. As for the proposed algorithm, the convergence tolerance ε is set to 0.001 and the discrete segments of state and decision variables are set to 11. The proposed algorithm is coded in GAMS 24.3, and each subproblem is solved by the MINOS (i.e., an NLP commercial solver) on a computer with i7-10700 CPU and 16GB memory.

The proposed method is compared with various methods in this section. According to [37] and [45], the errors of different methods can be calculated using:

$$e_s = \frac{F_s - F_s^*}{F_s^*} \tag{50}$$

$$e^{\mathrm{ave}} = \frac{1}{M}\sum_{s=1}^{M} e_s \tag{51}$$

where e_s represents the error of the compared method in the sth scenario; e^{ave} is the average error of the compared method; F_s represents the operational cost of the compared method in the sth scenario; while F_s^* represents the optimal operational cost (i.e., benchmark) in the sth scenario. It is obtained under the asesumption of accurate dispatch in each scenario.

A. Case of the 4-bus-4-node IEGS

The topology of the 4-node-4-bus IEGS is shown in Fig. 4, and the parameters are given in Tables III–V. The total installed capacity of the wind farm is 400 MW. Similar to [37], the exogenous information (i.e., the prediction errors of gas and electricity load, and wind power) are assumed to follow Gaussian distributions, in which the standard deviation of each exogenous information is 10% of its mean value. As shown in Fig. 5, 1000 sets of training scenarios and 100 sets of testing scenarios are sampled by MC simulation.

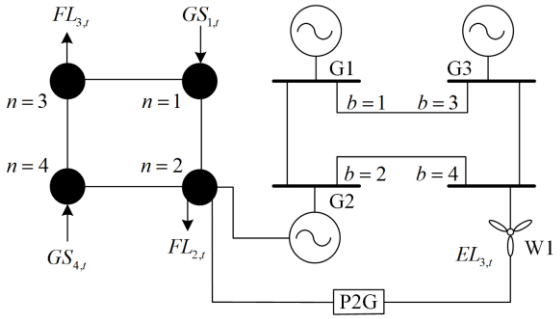

Fig. 4. Topology of the 4-node-4-bus IEGS.

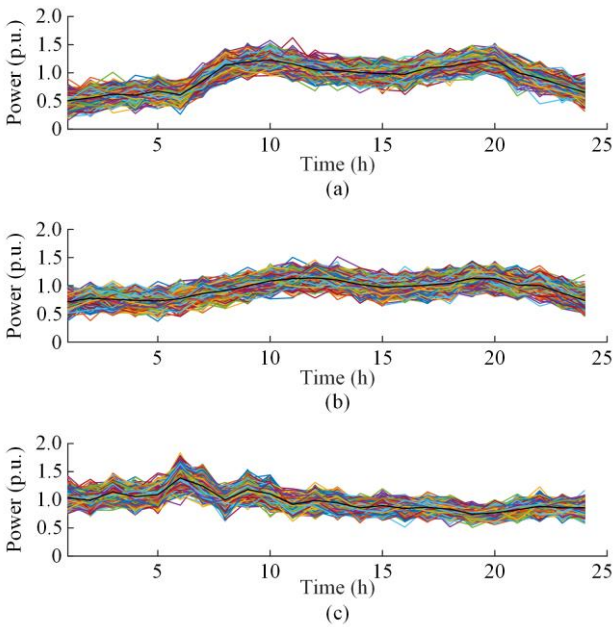

Fig. 5. Sampled scenarios. (a) Gas demand. (b) Electricity demand. (c) Wind power.

To demonstrate the advantage of the proposed risk-averse method, it is compared with the risk-neutral

method. In the proposed method, the risk-averse model is analyzed by algorithm 2, while in the risk-neutral method, the traditional risk-neutral model (i.e. (13)) is directly analyzed by the traditional lookup table-based ADP algorithm [37]. In order to accelerate the computation speed, the value functions of these two ADP algorithms are trained offline as described in Algorithm 2. The convergence processes of CVaR-ADP with different risk-averse preferences are shown in Fig. 6. It can be seen that CVaR-ADP is able to converge after about 190 iterations (i.e., within 5 minutes), regardless of the choice of risk preference.

TABLE III
PARAMETERS OF NODE PRESSURES AND GAS SOURCES

Node	1	2	3	4
$\pi_m^{\min}$ (bar)	40	40	40	40
$\pi_m^{\max}$ (bar)	60	55	55	60
$\pi_{m,t}^{o}$ (bar)	45	44	44	46
μ_m ($/Mm^3)	10 000			8000
$G_{\max}^{S}$ (Mm^3/h)	3			3.5
$G_{\min}^{S}$ (Mm^3/h)	0			0

TABLE IV
PARAMETERS OF CONSTANTS

Parameters	Values	Parameters	Values
C_{mn} ($/MWh)	10 000	η_{P2G} (Mm^3/MW)	0.005
W_{mn} (Mm^3/bar·h)^2	1.2268	C_{g}^{P} ($/MWh)	100 000
K_{mn} (Mm^3/bar)	0.3424	C_{e}^{P} ($/MWh)	10 000
η_{NG} (Mm^3/MW)	0.01	C_{w}^{P} ($/MWh)	1000

TABLE V
PARAMETERS OF GENERATORS

Generator	G1	G2	G3
$\text{P}_{\min}^{\text{G}}$ (MW)	50	50	50
$\text{P}_{\max}^{\text{G}}$ (MW)	200	300	250
b_i /($/MW·h)	75		70

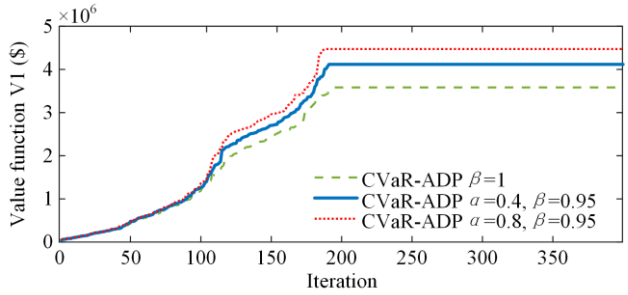

Fig. 6. Convergence processes of CVaR-ADP in the 4-bus-4-node IEGS.

Table VI takes the value function at period 1 as an example to illustrate the changes of convergence results with different risk preferences. When the risk preferences are set to $\alpha = 0.8$ and $\beta = 0.95$, the CVaR-VF at period 1 is \$ 4.473×10^6. When the risk preferences are adjusted to $\alpha = 0.4$ and $\beta = 0.95$, the CVaR-VF changes to \$ 4.116×10^6 accordingly. The reason is that the larger α and β are, the more conservative the decision is. In this way, the CVaR-VF can be trained under different risk preferences, which can then be applied in the real-time decision-making stage to speed up the method.

Table VII shows the comparison of the proposed risk-averse method and the risk-neutral method. Although the average cost of the proposed method is slightly larger than that of the risk-neutral method, the CVaR cost of the proposed method is much smaller than that of the risk-neutral method. The greater the risk preference coefficients, the more obvious are the advantages of the proposed method over the risk-neutral method. This is because the proposed method can consider the tail risk, which facilitates the reduction of the risk cost in extreme scenarios.

TABLE VI
OFFLINE TRAINING RESULTS IN THE 4-BUS-4-NODE IEGS

Algorithm	CVaR-VF at period 1 ($)	CPU time (s)
CVaR-ADP ($\alpha = 0.8, \beta = 0.95$)	4.473×10^6	269.73
CVaR-ADP ($\alpha = 0.4, \beta = 0.95$)	4.116×10^6	265.88
CVaR-ADP ($\beta = 1$)	3.583×10^6	189.88

TABLE VII
REAL-TIME OPTIMIZATION RESULTS IN THE 4-BUS-4- NODE IEGS

Method	Average cost ($)	95%CVaR cost ($)	Average error (%)
Risk-averse ($\alpha = 0.8, \beta = 0.95$)	3.661×10^6	4.618×10^6	0.166
Risk-averse ($\alpha = 0.4, \beta = 0.95$)	3.685×10^6	4.834×10^6	0.463
Risk-neutral	3.579×10^6	5.219×10^6	1.871

In Figs. 7 and 8, the results in an extreme scenario are taken as an example to illustrate the differences between the proposed risk-averse method and the risk-neutral method. As Fig. 8(a) depicts, the results provided by the proposed risk-averse method (corresponding $\alpha = 0.8$ and $\beta = 0.95$) have three line pack peaks. The first can absorb surplus wind power, while the second and third can provide sufficient power supply for the later peak loads. Therefore, there is no load shedding and wind power curtailment, as shown in Fig. 8(b). However, it can be seen from Fig. 9(a) that there are only two line pack peaks when the risk-neutral method is applied. Because of the lack of line pack, the result of the risk-neutral method exhibits a certain degree of load shedding in load peak periods, as shown in Fig. 9(b). Thus, the CVaR cost of the risk-neutral method is higher than that of the proposed method.

In terms of calculation time, since the well-trained value functions are used in both methods, the iterative calculation in the real-time optimization dispatch stage can be avoided effectively. Therefore, the decisions can be made within 0.2 s in both methods.

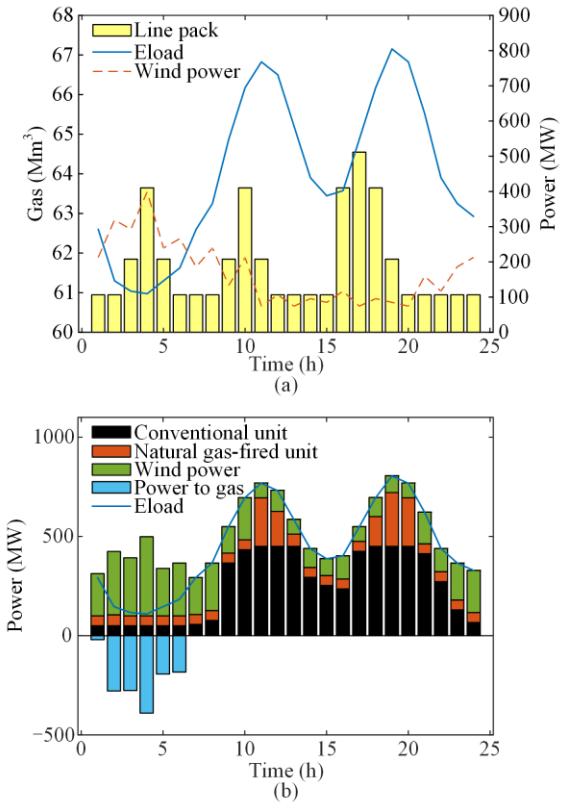

Fig. 7. Real-time optimization results of the risk-averse method in the 4-bus-4-node IEGS. (a) Gas dispatch results. (b) Power dispatch results.

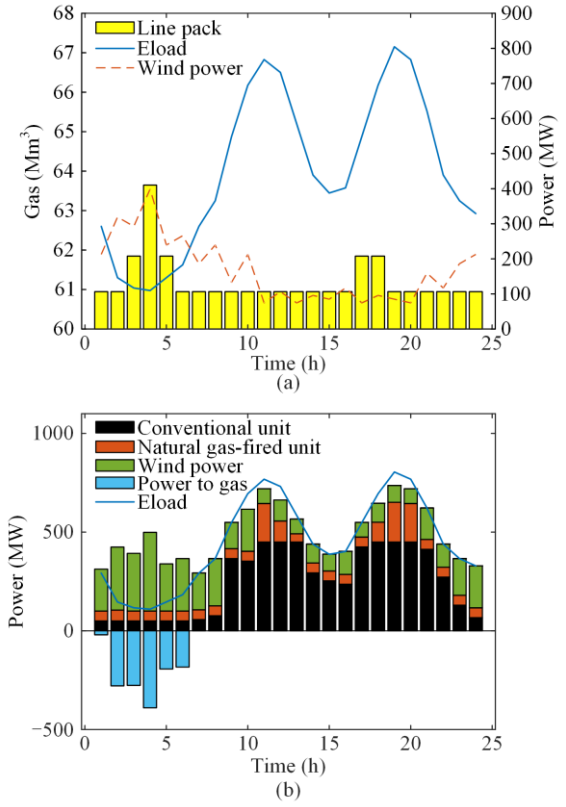

Fig. 8. Real-time optimization results of the risk-neutral method in the 4-bus-4-node IEGS. (a) Gas dispatch results. (b) Power dispatch results.

B. Case of the 39-bus-20-node IEGS

To illustrate the effectiveness of the proposed risk-averse method, further comparisons with more methods (i.e., the risk-neutral method, myopic policy and MPC) are carried out on a modified IEEE-39-bus-Belgian -20-node IEGS [44] depicted in Fig. 9. The parameters are given in Tables VIII and IX. The total installed capacities of conventional units, natural gas units, and wind farm are 6000 MW, 6000 MW, and 12 000 MW, respectively. Similar to the previous test, the exogenous information (i.e., the prediction errors of gas and electricity load, and wind power) are also assumed to follow Gaussian distributions, and the standard deviation of each exogenous information is 10% of the mean value. In the tests, 1000 sets of training scenarios and 100 sets of testing scenarios are sampled by MC simulation. In addition, the risk preferences are set to $\alpha = 0.8$ and $\beta = 0.95$.

TABLE VIII
PARAMETERS OF NODE PRESSURES AND GAS SOURCES IN THE 20-NODE SYSTEM

Node	$\pi_m^{\min}$ (bar)	$\pi_m^{\max}$ (bar)	$\pi_{m,t}^{o}$ (bar)	μ_m ($/Mm^3)	$G_{\max}^{S}$ (Mm^3/h)	$G_{\min}^{S}$ (Mm^3/h)
1	60	35	40	7000	10	0
2	60	35	40			
3	60	35	40			
4	60	35	40			
5	60	35	40	6500	10	0
6	60	35	40			
7	60	35	40			
8	60	35	40	6500	8	0
9	60	35	40			
10	60	35	40			
11	60	35	40			
12	60	35	40			
13	60	35	40			
14	60	35	40			
15	60	35	40			
16	60	35	40	7500	10	0
17	60	35	40			
18	60	35	40			
19	60	35	40			
20	60	35	40	7000	8	0

TABLE IX
PARAMETERS OF GENERATORS IN THE 39-BUS SYSTEM

Bus	$P_{\max}^{G}$ (Mm^3/h)	$P_{\min}^{G}$ (Mm^3/h)	b_i (Mm^3/h)
30	100	1000	70
31	100	1000	
34	100	1500	75
36	100	1000	
37	100	1500	70
38	100	1000	
39	100	1000	

Myopic policy simply considers the optimality of the current period, while MPC uses the forecast information of the following 4 periods. For the proposed risk-averse and risk-neutral methods, the value functions of the proposed CVaR-ADP algorithm and the traditional ADP algorithm are also trained offline beforehand, and the convergence processes are shown in Fig. 10.

Table X shows the optimization results of different methods in the real-time dispatch stage. Compared with traditional real-time methods (i.e., the myopic policy and MPC), the proposed method can reduce the optimization errors to some extent. It can also be seen that both the average cost and CVaR cost of the proposed method are smaller than those of myopic policy and MPC. This is because the proposed method can overview all optimization periods, while the other two only use the information of the current period or the following four periods.

Although the calculation time of the proposed method is longer than that of the myopic policy method, the decisionsc an still be finished within 10 s. Considering that the average time shown in Table 6 is the sum of the decision times of 24 periods, the calculation time to obtain the optimal decision for each period is 1/24 of the data in Table VI. Therefore, the proposed algorithm can meet well the requirement for real-time dispatch of an IEGS.

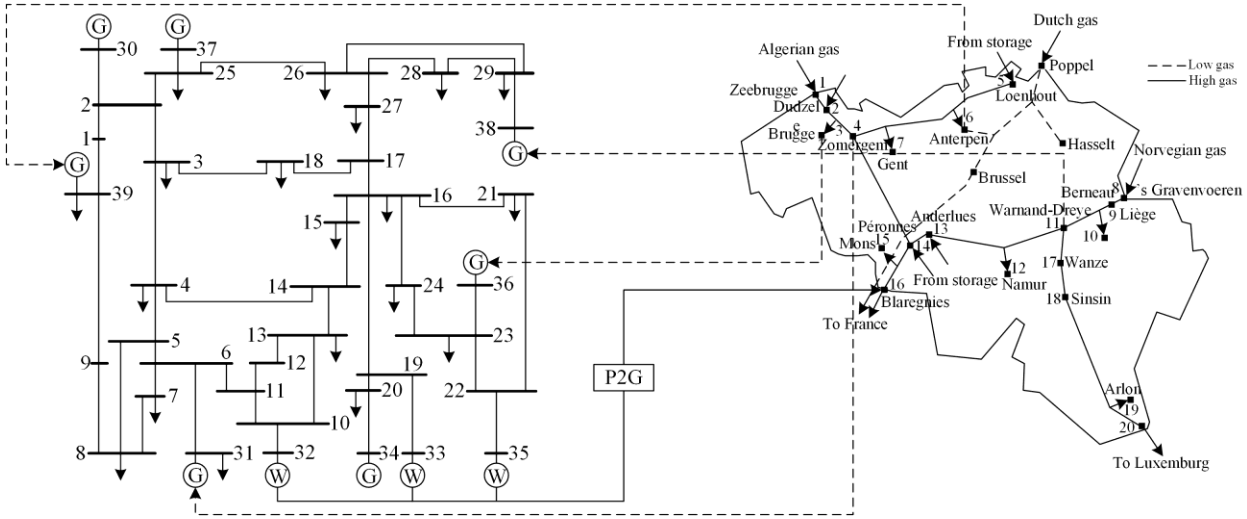

Fig. 9. Topology of the 39-bus-20-node IEGS.

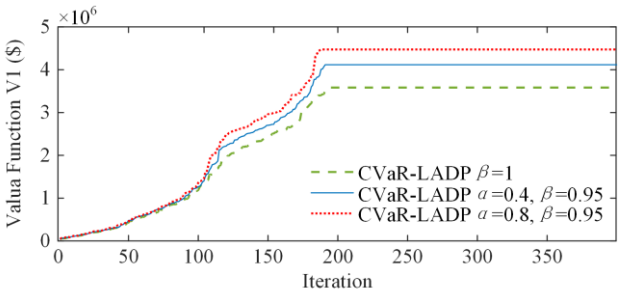

Fig. 10. Convergence processes of CVaR-ADP in the 39-bus-20-node IEGS.

TABLE X
REAL-TIME OPTIMIZATION RESULTS IN THE 39-BUS-20-NODE IEGS

Method	95% CvaR cost ($)	Average cost ($)	Average error (%)	Average time (s)
Risk-averse	8.955×10^7	7.977×10^7	0.362	10
Risk-neutral	10.337×10^7	7.897×10^7	2.737	10
MPC	11.146×10^7	8.186×10^7	3.394	12
Myopic	13.364×10^7	8.458×10^7	12.437	1

V. CONCLUSION

This paper proposes a risk-averse real-time dispatch model for the real-time operation of an IEGS with uncertainties. This is analyzed using a CVaR-ADP algorithm. The main conclusions are:

1) The proposed method can effectively deal with the uncertainties according to the risk preferences.

2) Compared with the traditional risk-neutral method, the proposed method is more favorable for reducing load shedding and wind power curtailment in extreme scenarios.

3) Compared with the myopic policy and MPC, the proposed method can obtain lower average cost and CVaR cost.

4) The proposed method reduces the CVaR cost, while increasing the average cost. In actual application, the operator of an IEGS should make real-time decisions according to its risk preference.

5) This paper focuses on a new ADP framework to deal with risk and uncertainty. The limitation of the proposed method is that the calculation of CVaR is based on the assumed distribution information, which may be difficult to acquire in practice. Therefore, it is intended to apply data-driven techniques to improve the applicability of the proposed method in future research. In addition, the proposed method will be extended to the decentralized optimization of multi-area IEGS.

ACKNOWLEDGMENT

Not applicable.

AUTHORS' CONTRIBUTIONS

Jianquan Zhu: He guided the study in the entire process and improved the text. Guanhai Li and Ye Guo: the idea, mathematical, practical design, case study and

writing the paper. Jiajun Chen, Haixin Liu, Yuhao Luo and Wenhao Liu: They reviewed and improved the text. All authors read and approved the final manuscript.

FUNDING

This work is supported by State Key Laboratory of HVDC under Grant SKLHVDC-2021-KF-09.

AVAILABILITY OF DATA AND MATERIALS

Not applicable.

DECLARATIONS

Competing interests: The authors declare that they have no known competing financial interests or personal relationships that could have appeared to influence the work reported in this article.

AUTHORS' INFORMATION

Jianquan Zhu received the B.S., M.S. and Ph.D. degrees in electrical engineering from Fuzhou University, Guangxi University, and Tsinghua University, in 2005, 2008, and 2012, respectively. He is currently an associate professor at the School of Electric Power Engineering, South China University of Technology, Guangzhou, China. His research interests are modeling and optimization of power systems.

Guanhai Li received the B.S. degree in electrical engineering from South China University of Technology, Guangzhou, China, where he is currently pursuing the M.S. degree. His research interests focus on applying approximate dynamic programming, optimization techniques and risk management in integrated energy system.

Ye Guo received the B.S. degree in electrical engineering from the South China University of Technology, Guangzhou, China, where he is currently working toward the M.S. degree. His research focuses on the computational intelligence and optimization of the integrated energy system.

Jiajun Chen received the B.S. degree in electrical engineering from South China University of Technology, Guangzhou, China, where he is currently pursuing the Ph.D. degree. His research interests focus on applying approximate dynamic programming and optimization techniques in power systems.

Haixin Liu received the B.S. degree in electrical engineering from South China University of Technology, Guangzhou, China, in 2018, where she is currently working toward the M.S. degree in electrical engineering. Her research interests focus on the computational intelligence and optimization of the integrated energy system.

Yuhao Luo received the B.S. degree in electrical engineering from South China University of Technology, Guangzhou, China, where he is pursuing the Ph.D. degree currently. His research interests focus on approximate dynamic programming and computational intelligence in power systems.

Wenhao Liu received the B.S. degree in electrical engineering from South China University of Technology, Guangzhou, China, where he is currently pursuing the M.S. degree. His research interests include power system economics and optimization.

REFERENCES

[1] B. Jia, D. Li, and X. Li *et al.*, "Two-stage restoration strategy for multi fault of an electric gas integrated energy system," *Power System Protection and Control*, vol. 50, no. 9, pp. 113-123, May 2022. (in Chinese)

[2] F. Qi, M. Shahidehpour, and F. Wen *et al.*, "Decentralized privacy-preserving operation of multi-area integrated electricity and natural gas systems with renewable energy resources," *IEEE Transactions on Sustainable Energy*, vol. 11, no. 3, pp. 1785-1796, Jul. 2020.

[3] L. He, Z. Lu, and J. Zhang *et al.*, "Economic dispatch of multi-area integrated electricity and natural gas systems considering emission and hourly spinning reserve constraints," *International Journal of Electrical Power & Energy Systems*, vol. 132, Nov. 2021.

[4] Z. Zhang, C. Wang, and S. Chen *et al.*, "Multitime scale co-optimized dispatch for integrated electricity and natural gas system considering bidirectional interactions and renewable uncertainties," *IEEE Transactions on Industry Applications*, vol. 58, no. 4, pp. 5317-5327, Jul. 2022.

[5] H. Khaloie, A. Anvari-Moghaddam, and J. Contreras *et al.*, "Offering and bidding for a wind producer paired with battery and CAES units considering battery degradation," *International Journal of Electrical Power & Energy Systems*, vol. 136, Nov. 2021.

[6] G. Zhang, F. Zhang, and K. Meng, "A distributed calculation method for robust day-ahead scheduling of integrated electricity-gas systems," *International Journal of Electrical Power & Energy Systems*, vol. 136, Mar. 2022.

[7] H. Golpîra, "Smart energy-aware manufacturing plant scheduling under uncertainty: a risk-based multi-objective robust optimization approach," *Energy,* vol. 209, Oct. 2020.

[8] D. Huo, C. Gu, and D. Greenwood *et al.*, "Chance-constrained optimization for integrated local energy systems operation considering correlated wind generation," *International Journal of Electrical Power & Energy Systems*, vol. 132, Nov. 2021.

[9] X. Liu, W. Wang, and Y. Zhang *et al.*, "Research on fat-tail phenomenon via artificial stock market modeling," *International Symposium on Computer Engineering and Intelligent Communications*, pp. 38-41, Aug. 2020.

[10] H. Khaloie, A. Abdollahi, and M. Rashidinejad *et al.*, "Risk-based probabilistic-possibilistic self-scheduling considering high-impact low-probability events uncertainty," *International Journal of Electrical Power & Energy Systems*, vol. 110, pp. 598-612, Sept. 2019.

[11] H. Khaloie, A. Anvari-Moghaddam, and N. D.Hatziargyriou *et al.*, "Risk-constrained self-scheduling of a hybrid power plant considering interval-based intraday demand response exchange market prices," *Journal of Cleaner Production*, vol. 282, Feb. 2021.

[12] H. Khaloie, F. Vallée, and C. S. Lai *et al.*, "Day-ahead and intraday dispatch of an integrated biomass-concentrated solar system: a multi-objective risk-controlling approach," *IEEE Transactions on Power Systems*, vol. 37, no. 1, pp. 701-714, Jan. 2022.

[13] A. Akbari-Dibavar, S. Nojavan, and B. Mohammadi-Ivatloo *et al.*, "Smart home energy management using hybrid robust-stochastic optimization," *Computers & Industrial Engineering*, vol. 143, May 2020.

[14] A. Al-Tamimi, F. L. Lewis and M. Abu-Khalaf, "Discrete-time nonlinear HJB solution using approximate dynamic programming: convergence proof," *IEEE Transactions on Systems, Man, and Cybernetics*, vol. 38, no. 4, pp. 943-949, Aug. 2008.

[15] S. Gorbachev, J. Guo, and A. Mani *et al.*, "MPC-based LFC for interconnected power systems with PVA and ESS under model uncertainty and communication delay," *Protection and Control of Modern Power Systems*, vol. 8, no. 4, pp. 1-17, Oct. 2023.

[16] A. Kirilenko, Y. Gong and C. Y. Chung, "A framework for power system operational planning under uncertainty using coherent risk measures," *IEEE Transactions on Power Systems*, vol. 36, no. 5, pp. 4376-4386, Sept. 2021.

[17] R. Rockafellar, and S. Uryasev, "Conditional value-at-risk for general loss distributions," *Journal of Banking & Finance*, vol. 26, no. 7, pp. 1443-1471, Sept. 2002.

[18] G. Wang and J. Luo, "Financing strategy of risk averse suppliers based on CVaR criterion," *Industrial Engineering and Management*, vol. 24, no. 4, pp. 55-63, Aug. 2019.

[19] D. Xiao, H. Chen, and W. Cai *et al.*, "Integrated risk measurement and control for stochastic energy trading of a wind storage system in electricity markets," *Protection and Control of Modern Power Systems,* vol. 8, no. 4, pp. 1-11, Nov. 2023.

[20] H. Golpîra and S. Khan, "A multi-objective risk-based robust optimization approach to energy management in smart residential buildings under combined demand and supply uncertainty," *Energy*, vol. 170, pp. 1113-1129, Mar. 2019.

[21] M. Tavakoli, F. Shokridehaki, and M. Akorede *et al.*, "CVaR-based energy management scheme for optimal resilience and operational cost in commercial building microgrids," *International Journal of Electrical Power & Energy Systems*, vol. 100, pp. 1-19, Sept. 2018.

[22] J. Yan, Y. Guo, and S. Zhang *et al.*, "Output current optimization for multibrick parallel discharge drivers based on genetic algorithm," *IEEE Transactions on Plasma Science*, vol. 47, no. 6, pp. 3015-3025, Jun. 2019.

[23] Y. Fu, Q. Sun, and R. Wennersten, "Effectiveness of the CVaR method in risk management in an integrated energy system," *Energy Reports*, vol. 6, pp. 1010-1015, Dec. 2020.

[24] Z. Chen, G. Zhu, and Y. Zhang *et al.*, "Stochastic dynamic economic dispatch of wind-integrated electricity and natural gas systems considering security risk constraints," *CSEE Journal of Power and Energy Systems*, vol. 5, no. 3, pp. 324-334, Sept. 2019.

[25] Z. Li, C. Wang, and B. Li, *et al.*, "Probability-interval-based optimal planning of integrated energy system with uncertain wind power," *IEEE Transactions on Industry Applications*, vol. 56, no. 1, pp. 4-13, Jan. 2020.

[26] M. Jadidbonab, E. Babaei, and B. Mohammadi-ivatloo, "CVaR-constrained scheduling strategy for smart multi carrier energy hub considering demand response and compressed air energy storage," *Energy*, vol. 174, pp. 1238-1250, May. 2019.

[27] J. Echanobe, K. Basterretxea, and I. d. Campo *et al.*, "Multi-objective genetic algorithm for optimizing an ELM-Based driver distraction detection system," *IEEE Transactions on Intelligent Transportation Systems*, vol. 23, no. 8, pp. 11946-11959, Aug. 2022.

[28] M. Sato, Y. Fukuyama, and T. Iizaka *et al.*, "Total optimization of energy networks in a smart city by multi-swarm differential evolutionary particle swarm optimization," *IEEE Transactions on Sustainable Energy*, vol. 10, no. 4, pp. 2186-2200, Oct. 2019.

[29] D. Garg and S. Devi, "RAP via hybrid genetic simulating annealing algorithm," *International Journal of System Assurance Engineering and Management*, vol. 12, pp. 419-425, Mar. 2021.

[30] GAMS development corporation: 'GAMS—the solver manuals, GAMS Development Corp.', NW, Washington, DC. Available at http:// www.gams.com/dd/docs/solvers/allsolvers.html, Jul. 2012.

[31] B. Cheng and W. B. Powell, "Co-optimizing battery storage for the frequency regulation and energy arbitrage using multi-scale dynamic programming," *IEEE Transactions on Smart Grid*, vol. 9, no. 3, pp. 1997-2005, May 2018.

[32] J. Nascimento and W. B. Powell, "An optimal approximate dynamic programming algorithm for concave, scalar storage problems with vector-valued controls," *IEEE Transactions on Automatic Control*, vol. 58, no. 12, pp. 2995-3010, Dec. 2013.

[33] J. Zhu, J. Chen, and Y. Zhuo *et al.*, "Stochastic energy management of active distribution network based on improved approximate dynamic programming," *IEEE Transactions on Smart Grid*, vol. 13, no. 1, pp. 406-416, Jan. 2022.

[34] J. Zhu, Y. Guo, and X. Mo *et al.*, "ADP-based decentralized algorithm for the optimal energy flow of the electricity–natural gas system," *IET Generation Transmission & Distribution*, vol. 14, no. 8, pp. 1528 -1539, Mar. 2020.

[35] D. Jiang and W. Powell, "Optimal hour-ahead bidding in the real-time electricity market with battery storage using approximate dynamic programming," *Informs Journal on Computing*, vol. 27, no. 3, pp. 525-543, Aug. 2015.

[36] Q. Sun, Z. Wu, and W. Gu *et al.*, "Flexible expansion planning of distribution system integrating multiple renewable energy sources: an approximate dynamic programming approach," *Energy*, vol. 226, Oct. 2021.

[37] H. Shuai, J. Fang, and X. Ai *et al.*, "Stochastic optimization of economic dispatch for microgrid based on approximate dynamic programming," *IEEE Transactions on Smart Grid*, vol. 10, no. 3, pp. 2440-2452, May 2019.

[38] H. Shuai, J. Fang, and X. Ai *et al.*, "Optimal real-time

operation strategy for microgrid: an ADP-based stochastic nonlinear optimization approach," *IEEE Transactions on Sustainable Energy*, vol. 10, no. 2, pp. 931-942, April 2019.

[39] Z. Wan, H. Li, and H. Shuai *et al.*, "Adversarial attack for deep reinforcement learning based demand response," *2021 IEEE Power & Energy Society General Meeting*, Washington, DC, 2021, pp. 1-5.

[40] A. Ruszczynski, "Risk-averse dynamic programming for Markov decision processes," *Math Program*, vol. 125: 235-261, June 2010.

[41] A. Shapiro, W. Tekaya, and J. Costa *et al.*, " Risk neutral and risk averse stochastic dual dynamic programming method," *European journal of operational research*, vol. 242, no. 2, pp. 375-391, Jan. 2013.

[42] C. M. Correa-Posada and P. Sánchez-Martín, "Integrated power and natural gas model for energy adequacy in short-term operation," *IEEE Transactions on Power Systems*, vol. 30, no. 6, pp.3347-3355, Nov. 2015.

[43] Y. Lu, H. Li, and Y. Liu *et al.*, "Optimal operation of electricity-gas-heat integrated energy system considering the risk of energy supply equipment failure," *Power System Protection and Control*, vol. 50, no. 9, pp. 113-123, May 2022. (in Chinese)

[44] S. Chen, A. J. Conejo, and R. Sioshansi *et al.*, "Operational equilibria of electric and natural gas systems with limited information interchange," *IEEE Transactions on Power Systems*, vol. 35, no. 1, pp. 662-671, Jan. 2020.

[45] R. Khodabakhsh and S. Sirouspour, "Optimal control of energy storage in a microgrid by minimizing conditional value-at-risk," *IEEE Transactions on Sustainable Energy*, vol. 7, no. 3, pp. 1264-1273, Jul. 2016.

[46] W. B. Powell and S. Meisel, "Tutorial on stochastic optimization in energy part I: modeling and policies," *IEEE Transactions on Power Systems*, vol. 31, no. 2, pp. 1459-1467, Mar. 2016.